Optics & Laser Technology 164 (2023) 109491

Contents lists available at ScienceDirect

Optics and Laser Technology

journal homepage: www.elsevier.com/locate/optlastec

Full length article

Fourier series diffractive lens with extended depth of focus

Angela Soria-Garcia [a], Luis Miguel Sanchez-Brea [a,*], Jesus del Hoyo [a], Francisco Jose Torcal-Milla [b], Jose Antonio Gomez-Pedrero [c]

[a] Applied Optics Complutense Group, Optics Department, Faculty of Physics, Universidad Complutense de Madrid, Plaza de las Ciencias, 1, 28040, Madrid, Spain
[b] Applied Physics Department, Grupo de Tecnología Óptica Láser, Instituto de Investigación en Ingeniería de Aragón (i3a), Universidad de Zaragoza, C/ Pedro Cerbuna 12, 50009, Zaragoza, Spain
[c] Applied Optics Complutense Group, Optics Department, Faculty of Optics and Optometry, Universidad Complutense de Madrid, C/ Arcos de Jalón, 118, 28037, Madrid, Spain

ARTICLE INFO

Keywords:
Diffractive lenses
Diffractive optical elements
Extended depth of focus
Fourier series

ABSTRACT

Angular diffractive lenses have been proven to achieve a narrow beam waist with a long depth of focus. We generalize these type of lenses by defining the angular distribution of the focal length as a Fourier series. The Fourier coefficients of the lens are optimized, using Particle Swarm Optimization algorithm, to minimize the beam width and increase its uniformity for a given depth of focus. In order to obtain a fast simulation during the optimization process, we used Chirp Z-transform algorithm. Finally, we performed an experimental verification of the results using a Spatial Light Modulator. The Fourier series diffractive lens presents a more uniform and narrower beam than previous angular lenses, in both simulations and experiments. These results may find applications in the design of contact and intraocular lenses with extended depth of focus, laser focusing and imaging systems.

1. Introduction

Optical imaging systems normally require a wide focusing range with reliable resolution. Conventional refractive lenses can achieve a narrow beam waist when they have high numerical aperture, with the disadvantage that there is a sharp reduction in depth of focus. Trying to solve the problem of narrow depth of focus, diffractive elements with extended depth of focus (EDOF) have been proposed. Such elements are useful in a range of applications. In microscopy [1,2], where high numerical aperture is required to achieve good resolution, EDOF lenses allow to relax the mechanical restrictions of the system and, thus, the complexity and cost. Material laser processing techniques also benefit from an EDOF lens, again by relaxing the mechanical constrains in the laser positioning. In addition, it is also possible to shape the laser beam to obtain specific properties of the processed materials [3]. Other field in which EDOF lenses have found application is in the design of new contact and intraocular lenses for compensating presbyopia [4–7]. In this case, EDOF lenses allow the presbyopic patient to enhance the depth of focus of the eye, focusing objects placed at different distances in a similar way as a not presbyopic subject does by means of ocular accommodation. Several types of optical elements have been proposed to enlarge the lenses depth of focus such as apodizers [8], computer generated holograms [9,10] or diffractive optical elements (DOEs) [11,12]. Within the last group, it is quite common to combine conventional refractive lenses with amplitude or phase DOEs to achieve longer depth of focus. These DOEs can present a radial distribution, like axicons, axilenses or optical elements with a certain number of rings [1,13,14]. Another possibility are the diffractive angular EDOF lenses. Daschner et al. proposed the Daisy lens, which presents a sinusoidal angular variation of the focal length, producing a dual focus intensity distribution [15,16]. Sabatyan and Golbandi proposed the petal-like lens which still generate a dual focus intensity distribution [17,18]. Nevertheless, for Daisy and petal-like lenses, when both focii are close enough, the intensity distribution is similar to an elongated focus. A better design to obtain extended depth of focus is the Lotus lens [19,20], where the focal length variation is linear, instead of sinusoidal. However, diffractive effects still produce a certain non-uniformity at the intensity distribution around the focusing area. As a consequence, the Sector-based Fresnel zone plate (SFZP) was defined to slightly modify the histogram distribution of the focal length variation, including quadratic and cubic terms [21].

In the present work, we improve the behavior of previous EDOF lenses, and propose the most general angular diffractive lens, where the angular variation of the focal length is defined as a Fourier series. As the number of degrees of freedom is greatly increased, optimization techniques must be used to obtain the Fourier coefficients of the lens [2,12,22,23]. The optimization procedures are mainly devoted to reduce

* Corresponding author.
E-mail addresses: angsoria@ucm.es (A. Soria-Garcia), optbrea@ucm.es (L.M. Sanchez-Brea), jhoyo@ucm.es (J. del Hoyo), fjtorcal@unizar.es (F.J. Torcal-Milla), jagomezp@ucm.es (J.A. Gomez-Pedrero).

https://doi.org/10.1016/j.optlastec.2023.109491
Received 1 February 2023; Received in revised form 18 March 2023; Accepted 11 April 2023
Available online 24 April 2023

the beam width, while maintaining the uniformity of the beam. With this purpose, using Particle Swarm Optimization algorithm [24,25], we select the optimal Fourier coefficients in terms of the wavelength, mean focal length, diameter of the lens, and desired depth of focus (DOF). In addition, we perform an experimental verification of the FSDL using a Spatial Light Modulator (SLM).

2. Definition of the Fourier series diffractive lens

Let us consider an aberration-corrected standard lens illuminated by a monochromatic and collimated Gaussian beam. The main parameters of its focus are the beam width and the depth of focus, which are interrelated since a small value of the beam waist, $2\omega_0$, gives a small value of DOF and vice-versa [26],

$$\omega_0 = \frac{2\lambda}{\pi}\left(\frac{f'}{D}\right), \tag{1}$$

$$DOF = \frac{2\pi\omega_0^2}{\lambda} = \frac{8\lambda}{\pi}\left(\frac{f'}{D}\right)^2, \tag{2}$$

where λ is the wavelength of the beam, D is the diameter of the lens and f' is the lens focal length.

As we can see, when we try to increase the DOF, reducing the lens diameter or increasing the focal length, the focal width is also increased. Angular lenses are an alternative to standard lenses, since they do not present the previous restrictions. They are defined in a similar way, but with a periodical angular focal length variation. Their transmittance is given by [20]

$$t_G(r,\theta) = P(r)\,exp\left[-ik\frac{r^2}{2g\,(M\cdot\theta)}\right], \tag{3}$$

where $k = 2\pi/\lambda$ is the wavenumber, r and θ are the radial and angular coordinates, $g\,(\theta)$ is a periodic function in $\theta \in [0, 2\pi]$ which generates the angular focal variation, M is the number of periods in the 2π range (number of petals) [17], $P(r)$ represents the pupil function of the lens

$$P(r) = \begin{cases} 1 & r \le R, \\ 0 & r > R, \end{cases} \tag{4}$$

and R is the radius of the lens.

One of the first angular lenses was the Daisy lens, which presents a sinusoidal angular variation of the focal length with discrete symmetry [19]

$$g_D(\theta) = f' + \frac{\Delta f}{2}sin\,(\theta), \tag{5}$$

where f' is the mean focal length, and Δf represents the design DOF length. The minimum and maximum focal values are $f' - \Delta f/2$ and $f' + \Delta f/2$, respectively. A Daisy lens with low Δf produces a beam similar to an elongated focus, but with higher Δf it still generates a dual-focus intensity distribution. In order to improve the performance of this lens and obtain a uniform and extended focus, the Lotus lens was proposed [20], which presents a linear focal length distribution,

$$g_L(\theta) = f' + \frac{\Delta f}{2}\left[4\left|\frac{\theta}{2\pi} - \text{floor}\left(\frac{\theta}{2\pi} + \frac{1}{2}\right)\right| - 1\right], \tag{6}$$

where floor(·) represents the floor function (round to the nearest integer lower than the function argument). Although the histogram of $g_L(\theta)$ is linear between $f' - \Delta f/2$ and $f' + \Delta f/2$, diffractive effects produce a non-uniform focal intensity distribution. As a consequence, sectorized Fresnel zone plate (SFZP) was proposed [21], where the histogram of the focal length is not linear, but quadratic and cubic terms are added,

$$f_i = (1 - k_1 - k_2)f_{1,i} + k_1 f_{2,i} + k_2 f_{3,i}, \tag{7}$$

with

$$f_{1,i} = (f' - \Delta f/2) + \Delta f\frac{i}{n_f}, \tag{8}$$

$$f_{2,i} = (f' - \Delta f/2) + \Delta f\left(\frac{i}{n_f}\right)^2,$$

$$f_{3,i} = f' + 4\Delta f\left(\frac{i - n_f/2}{n_f}\right)^3.$$

In these equations, i represents a certain sector and n_f is the total number of sectors. The effect of these quadratic and cubic terms is controlled by two parameters, k_1 and k_2, which are optimized in order to obtain a more uniform focal intensity distribution.

In this work, we present a different approach to improve the performance of EDOF lenses. As we are studying lenses with angular symmetry, we generalize them as a cosine Fourier series, which is described as

$$g_F(\theta) = f' + \frac{\Delta f}{2}\sum_{l=1}^{L} a_l \cos(l\cdot\theta), \tag{9}$$

where l corresponds to the Fourier coefficients order and a_l represents their values which are calculated according to

$$a_l = \frac{1}{\pi}\int_0^{2\pi} g_F(\theta)\ \cos(l\cdot\theta)\ d\theta. \tag{10}$$

As an example, Fig. 1 shows a standard lens and a Fourier Series Diffractive Lens (FSDL) with $D = 4$ mm and $f' = 250$ mm. The FSDL is designed with a depth of focus of $\Delta f = 25$ mm and five non-zero Fourier coefficients. Also, a scheme of the expected behavior of the FSDL, compared to that of a standard Fresnel lens, is shown.

As Eq. (9) is the most general case for angular lenses, Daisy and Lotus lenses are included in this kind of Fourier series representation. The coefficients for the Daisy lens are

$$a_l^1 = \begin{cases} 0.5 & l = 1, \\ 0 & l \ne 1. \end{cases} \tag{11}$$

The coefficients for the Lotus lens are

$$a_l^1 = \begin{cases} \frac{8}{(l\pi)^2} & l \text{ odd}, \\ 0 & l \text{ even}. \end{cases} \tag{12}$$

The SFZP also presents a Fourier series representation. For better comparison, we will compute the Fourier coefficients of the equivalent phase lens (not the binarized version). The Fourier coefficients of this lens are

$$a_l = (1 - k_1 - k_2)a_l^1 + k_1 a_l^2 + k_2 a_l^3, \tag{13}$$

where a_l^1 are the same as those of Lotus lens, and the quadratic and cubic coefficients are

$$a_l^2 = \frac{8}{(l\pi)^2}\ \forall l, \tag{14}$$

$$a_l^3 = \begin{cases} \frac{-6}{l^4\pi} + \frac{3\pi}{4l^2} & l \text{ odd}, \\ 0 & l \text{ even}. \end{cases} \tag{15}$$

The Fourier coefficients given in Eq. (13) depend on k_1 and k_2 parameters, and they need to be optimized for each lens design. In Section 3, we will use these coefficients as seeds for the optimization process of FSDL.

Once the FSDL is defined, we calculate the intensity distribution around the focus using a numerical approach based on Rayleigh-Sommerfeld equation [27]. In order to obtain fast and accurate results, we use Chirp Z-transform algorithm (CZT), also called Bluestein method [28,29]. With CZT, the region of interest (number and size of pixels) can be selected and it is not fixed by the resolution of the initial field. Since the focal region is very small compared to the lens size, the focal intensity distribution can be properly sampled with a much lower computing time and memory usage than with the standard Rayleigh-Sommerfeld algorithm [30].

For the simulations, we need to set the maximum number of Fourier coefficients, $L = \max(l)$, that influence the lens performance. For this, we have determined the beam width of a Fourier lens whose coefficients are those shown in Eq. (13). As an example, the parameters

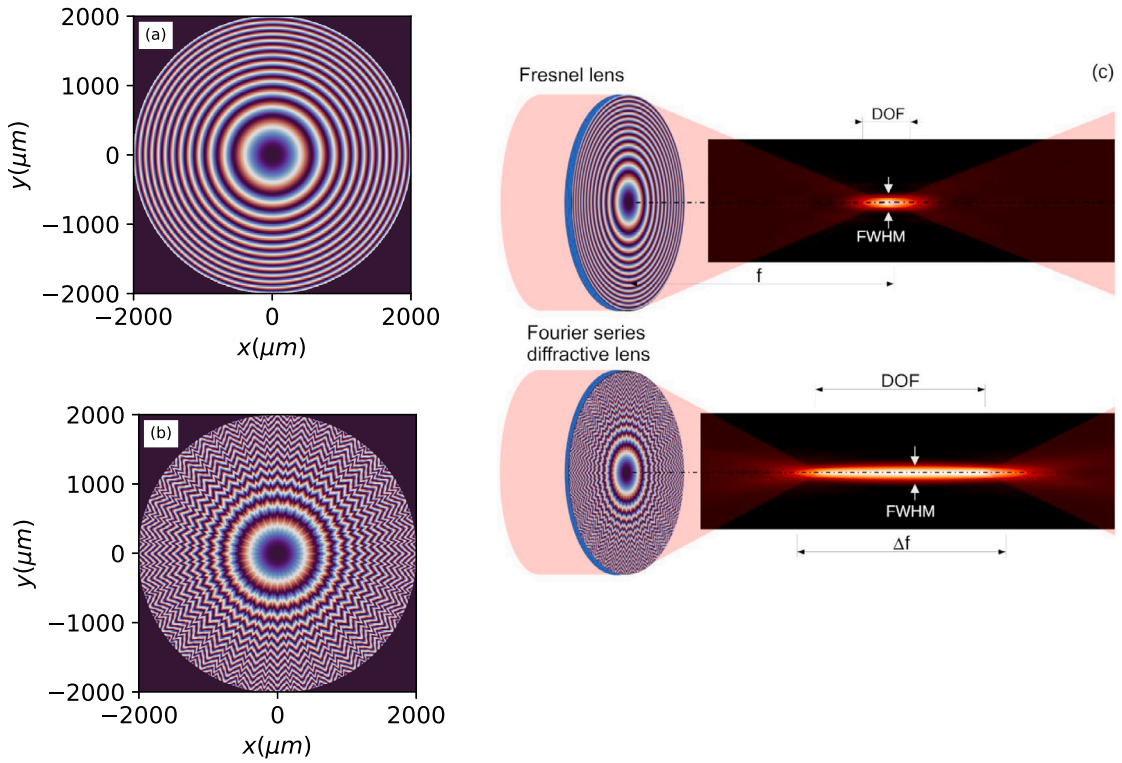

Fig. 1. Phase maps of (a) Fresnel and (b) FSDL lens with $D = 4$ mm and $f' = 250$ mm. The FSDL presents a depth of focus $\Delta f = 25$ mm and 5 Fourier coefficients: $a_l = [0.9, 0.7, -0.2, 0.3, -0.1]$. (c) Optical scheme for the Fresnel lens and the FSDL, including the expected results for extended depth of focus. The intensity distribution for the FSDL is obtained with coefficients of Table 1a.

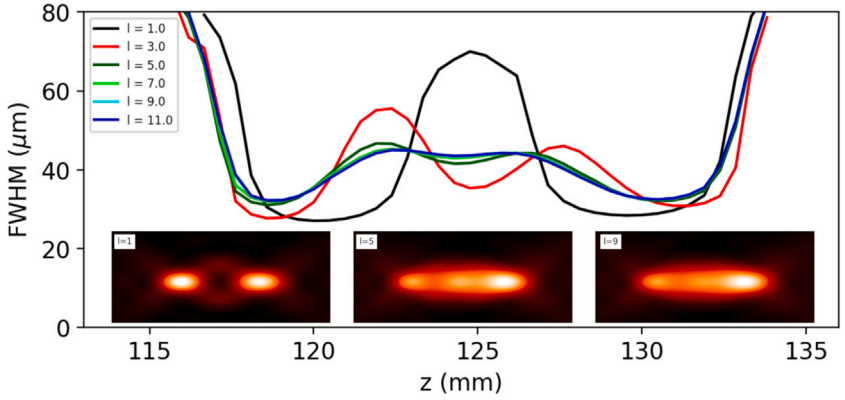

Fig. 2. Beam width, computed as FWHM, for a Fourier lens (whose Fourier coefficients are obtained using Eq. (13)) in terms of the number of Fourier coefficients. At the bottom of the figure, we show the intensity distribution XZ, obtained by numerical CZT approach, when $L = 1$, $L = 5$, and $L = 9$. The illumination is a plane wave with $\lambda = 632.8$ nm and the lens has a diameter $D = 4$ mm, focal length $f' = 125$ mm, and $\triangle f = 12.5$ mm.

of the lens studied are $f' = 125$ mm, $D = 4$ mm and $\Delta f = 12.5$ mm. We calculate the Full Width at Half Maximum (FWHM) for different number of coefficients. Fig. 2 shows that the beam width stabilizes with $L = 9$. Although this value may depend on the lens parameters, we have checked that $L = 9$ is valid for all the simulations performed in this work. This value is high enough so that the beam width stabilizes and, also, it is small enough to avoid manufacturing issues and to reduce the optimization process time.

3. Numerical analysis and optimization

The FSDL represents a generalization of angular lenses and, depending on the value of their coefficients, many types of focii can be produced. Since our objective is to obtain narrow, long, and homogeneous focal distributions, we need to find out the appropriate Fourier coefficients. For this, we have used an efficient and quick optimization algorithm, Particle Swarm Optimization (PSO) [24,25]. It is a metaheuristic optimization algorithm based on a population of particles, whose movement is influenced by its best local position but it is also guided towards the best global position, which is constantly updated by the rest of the particles (swarm). The movement of the particles around the search space is ruled by two equations, the velocity of each particle of the swarm and its position

$$v_{i,j}^{(k+1)} = \omega\, v_{i,j}^{(k)} + c_1 r_1^{(k)} \left(p_{i,j}^{(k)} - x_{i,j}^{(k)}\right) + c_2 r_2^{(k)} \left(g_j^{(k)} - x_{i,j}^{(k)}\right), \tag{16}$$

$$x_{i,j}^{(k+1)} = x_{i,j}^{(k)} + v_{i,j}^{(k+1)}, \tag{17}$$

where the indexes i, j, k represent the number of particles, dimensions and iterations respectively. The first one has an inertial component

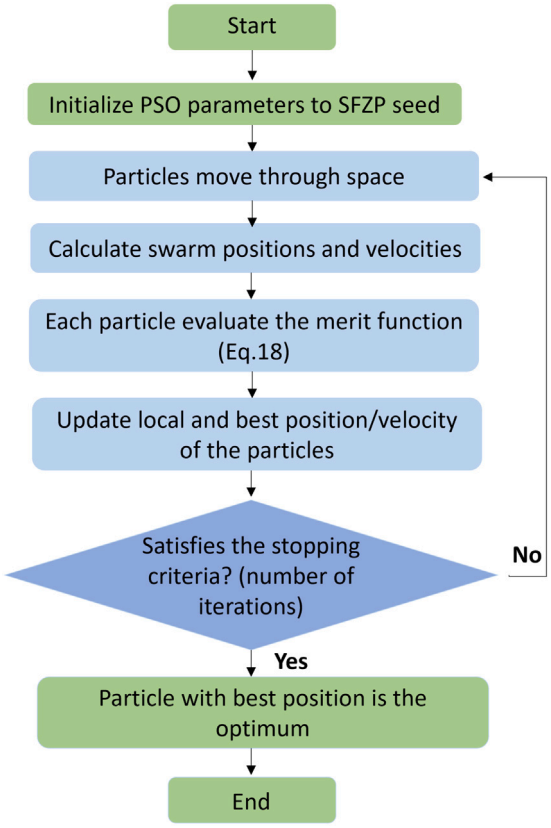

Fig. 3. Flow chart of particle swarm optimization. First, we initialize the optimization process using SFZP seed. Then, the position and velocity of the particles are constantly being updated to minimize the merit function. The algorithm finishes when the set number of iterations is reached, and the solution is given by the particle with the best position.

which depends on the velocity at the previous instant, a cognitive term which directs the particle to the best local position and a social term which leads the particle to the best global position. In Eq. (16), ω corresponds to the inertia weight parameter, c_1 and c_2 are cognitive and social constants respectively, r_1 and r_2 are two random values set between [0, 1], $p_{i,j}$ represents the previous best position of each particle, and g_j indicates the global best position of the swarm. For computation, we have used a Python library called PySwarms [31], which allows solving optimization tasks intuitively. This library has implemented global-best PSO, local-best PSO, as well as a general optimizer for custom topologies.

3.1. Optimized Fourier series diffractive lens

Now, we analyze the viability of converting a FSDL into a EDOF lens through the optimization of its Fourier coefficients. As a first example, we have designed a FSDL with focal length $f' = 125$ mm, diameter $D = 4$ mm and $\lambda = 633$ nm for two cases: $\Delta f = 12.5$ mm and $\Delta f = 25$ mm.

The PSO algorithm needs a seed for the initial values of the Fourier coefficients. Random seed coefficients can be used in the optimization algorithm. However, we found that the algorithm does not always converge to an optimal solution since many local minima exist. As a consequence, we opted to provide the optimized coefficients of the SFZP lens as the initial values, Eq. (13), since, to our knowledge, it is the best EDOF angular lens up-to-date. The seed coefficients used for the two example lenses, $\Delta f = 12.5$ mm and $\Delta f = 25$ mm, are shown in Table 1 (Initial column). Then, we have performed a PSO process to optimize the Fourier coefficients of the FSDL (see flow chart of Fig. 3). We used L = 9 degrees of freedom, 20 particles and 10 iterations. We

Table 1
Fourier coefficients before and after optimization for FSDL with (a) $\Delta f = 12.5$ mm and (b) $\Delta f = 25$ mm.

(a)			(b)		
a_l	Initial	Optimized	a_l	Initial	Optimized
a_1	0.7632	0.7133	a_1	0.7468	0.6363
a_2	−0.0162	0.0031	a_2	−0.0073	0.0133
a_3	0.1093	0.1142	a_3	0.116	0.1008
a_4	−0.0040	0.0006	a_4	−0.0018	0.0033
a_5	0.0400	0.0398	a_5	0.0427	0.0400
a_6	−0.0018	0.0003	a_6	−0.0008	0.0019
a_7	0.0205	0.0241	a_7	0.0219	0.0214
a_8	−0.0010	0.0002	a_8	−0.0005	0.0008
a_9	0.0124	0.0112	a_9	0.0133	0.0178

also used bounds (± 20%) to the coefficients to prevent the particles to scatter too far from the initial values. At each iteration, we obtain the intensity distribution at several z-planes around its focal plane, and estimate the beam width, using FWHM. Then, we define the merit function as a sum of two terms

$$MF = \frac{\sqrt{\sum_{i=1}^{N}\left[I(x=0,y=0,z_i) - I_{obj}(x=0,y=0,z_i)\right]^2}}{N} + \alpha\frac{\sqrt{\sum_{i=1}^{N}\left[FWHM(z_i) - FWHM_{obj}(z_i)\right]^2}}{N}. \tag{18}$$

The first term is related to uniformity of the intensity distribution at axis and the second term minimizes the beam width (given by FWHM), being α a balance factor that, in the examples presented is $\alpha = 1$. In this function, I_{obj} is the target intensity distribution

$$I_{obj} = \begin{cases} 1 & z\,\epsilon\,\left[f' - \Delta f/2, f' + \Delta f/2\right], \\ \frac{1}{1+\beta^2(z-z_1)^2} & z < f' - \Delta f/2, \\ \frac{1}{1+\beta^2(z-z_2)^2} & z > f' - \Delta f/2, \end{cases} \tag{19}$$

where $z_1 = f' - \Delta f/2$, $z_2 = f' + \Delta f/2$ and $\beta = 0.25$ is a parameter that controls the curve drop. This function simulates a beam whose axial intensity is completely uniform along its depth of focus. I is the normalized intensity distribution and N is the total number of measures. On the other side, $FWHM_{obj}$ corresponds to a beam with the desired width normalized along its depth of focus, which can be expressed as

$$FWHM_{obj} = \begin{cases} 1 & z\,\epsilon\,\left[f' - \Delta f/2, f' + \Delta f/2\right], \\ 1 - (z - z_1) & z < f' - \Delta f/2, \\ 1 + (z - z_2) & z > f' + \Delta f/2. \end{cases} \tag{20}$$

Fig. 4 shows the optimized intensity patterns and Table 1 the optimized coefficients (Optimized column). The beam width and, especially, the uniformity have been improved significantly. In fact, for the lens with $\Delta f = 12.5$ mm, the average beam width reduces from 39.23 μm to 38 μm and the standard deviation is 38.18% lower after optimization. Respect to the lens with $\Delta f = 25$ mm, FWHM takes a value of 50.64 μm compared to the initial width of 53.01 μm and the standard deviation of the beam intensity decreases a 58.49% at the cost that the DOF length is 2.5 millimeters shorter than its initial value.

To check the results obtained with the FSDL, we have compared them with previous angular lenses such as the sectorized Fresnel zone plate (SFZP) and the Lotus lens. Fig. 5 shows a noticeable improvement in DOF lenses behavior since FSDL presents lower FWHM and standard deviation of the axial intensity. For the lens with $\Delta f = 12.5$ mm (upper row of Fig. 5) we observe that the Lotus lens generates a dual focus pattern, result enhanced by the SFZP. Nevertheless, FSDL presents a much lower FWHM at the beam center and as a consequence, it does not form two focii and generates a smooth intensity pattern along the direction of propagation. For the FSDL lens with $\Delta f = 25$ mm (see lower

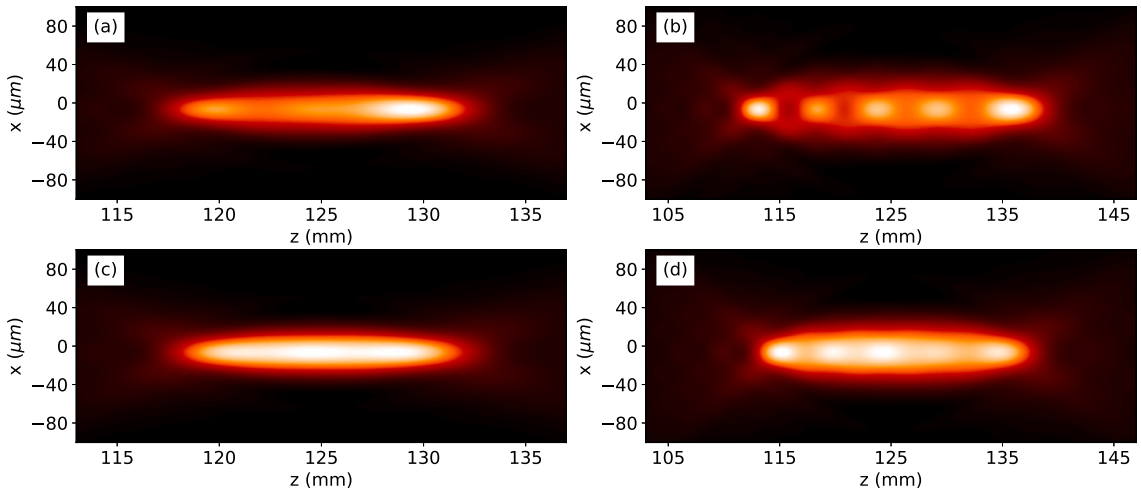

Fig. 4. Intensity distribution XZ around the focus of a FSDL with seed coefficients (upper row) and optimized coefficients (lower row). The intensity patterns obtained correspond to a FSDL with $f' = 125$ mm and $\Delta f = 12.5$ mm for (a) and (c), and $\Delta f = 25$ mm for (b) and (d).

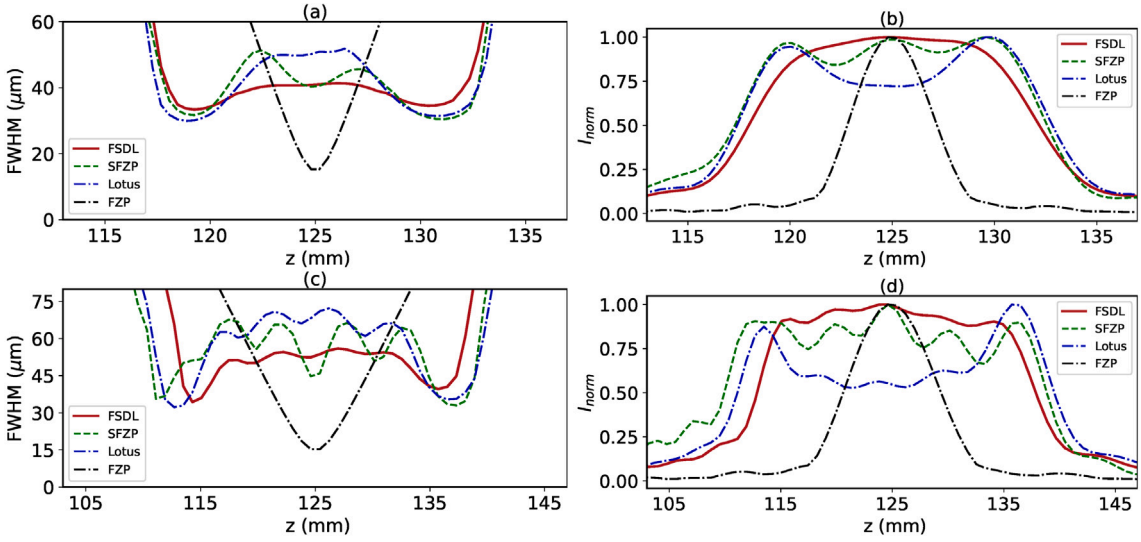

Fig. 5. (a, c) FWHM and (b, d) normalized intensity pattern along axis of several types of lenses (Fresnel Zone Plate (FZP), Lotus lens, SFZP, and FSDL) with (a, b) $\Delta f = 12.5$ mm and (c, d) $\Delta f = 25$ mm, respectively.

row of Fig. 5), the width and intensity fluctuation is greater than the FSDL with lower depth of focus. However, these parameters are still better than those of other EDOF lenses.

We have also checked the intensity distribution of the FSDL at the focal plane, $z = f$, and at distances $z = f \pm \Delta f/2$ for the case of Fig. 4c (Fig. 6a). We can see that the profile at the focal plane is similar to a Bessel profile, while at $z = f \pm \Delta f/2$ it is closer to a Lorentz profile. In order to analyze the focusing efficiency of the lens, we have also computed the encircled energy for these three profiles [32], and they have been compared to those of a Fresnel lens. We see that at focus, $z = f$, the Fresnel lens produces a narrower beam than the FSDL, but out of focus, $z = f \pm \Delta f/2$, the FSDL is much better than the Fresnel lens.

Finally, we study the dependence of beam width on Δf for Lotus lens, SFZP and FSDL. For this purpose, we design lenses with $f' = 125$ mm and different Δf, from 10 mm to 37 mm. We optimize their coefficients using the previous procedure, and determine the intensity distribution around the focus. Then, we calculate the average beam width for $f' - \Delta f/2 \leq z \leq f' + \Delta f/2$. Fig. 7a shows that the FWHM presents a square-root dependence with Δf. With the numerical data, we have plotted the fitting performed in dashed line and their 1σ error bands in shading. This fitting has been performed using Kriging, which is a family of best linear unbiased estimators in the minimal squared sense [33–35]. This figure also shows that the FSDL presents the lowest width beam for each Δf. Moreover, we analyze the behavior of the beam uniformity for these lenses (Fig. 7b). FSDL presents the best beam uniformity, especially for low Δf. The average standard deviation of the intensity patterns reaches values of 13.46%, 10.57% and 8.92% for Lotus, SFZP and FSDL, respectively, thus showing the improvement of FSDL over other EDOF lenses.

4. Experimental results

We have experimentally verified the performance of the designed FSDL using a SLM. A scheme of the set-up is shown in Fig. 8. A He–Ne laser with a working wavelength of $\lambda = 632.8$ nm and a Gaussian beam profile (Melles Griot, United States) has been used as light source. The beam has been filtered with a spatial filter and enlarged with a beam expander in order to illuminate the SLM as much as possible. For this purpose, we have used a 40x microscope objective, a 10 μm pinhole and a collimating lens. Then, the light beam goes through a polarizer (P_0) and a quarter-waveplate (QW_0) to change the light polarization from

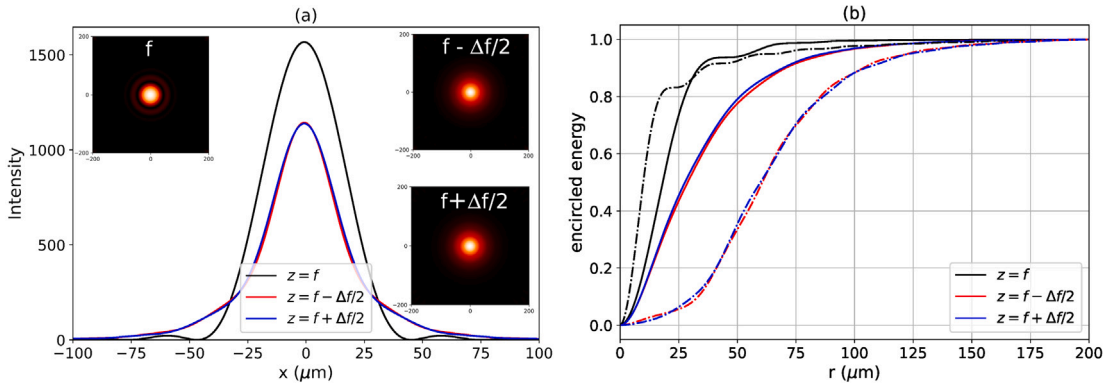

Fig. 6. (a) Intensity profiles at focus $I(x)$ at locations $z = f$, $z = f - \Delta f/2$, and $z = f + \Delta f/2$ for the lens of Fig. 4c and intensity distribution $I(x, y)$, respectively. (b) Normalized encircled energy for the FSDL (continuous line) and for the Fresnel lens (dash-dotted line).

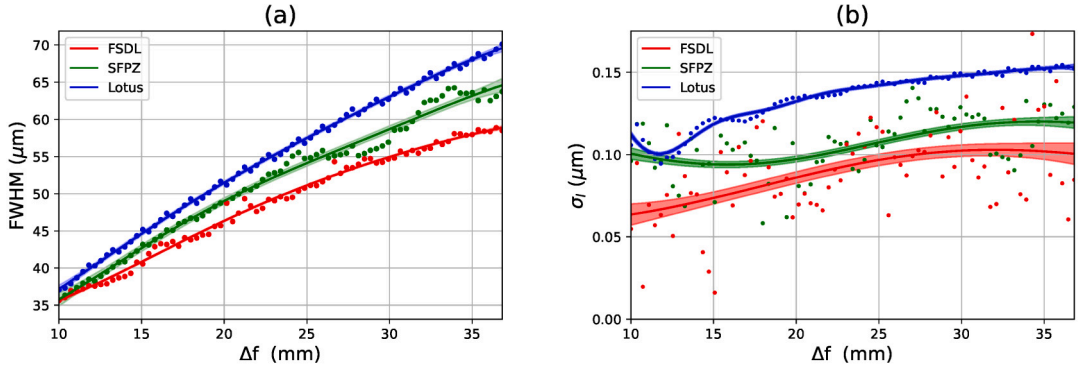

Fig. 7. (a) FWHM and (b) standard deviation of the axis intensity as a function of depth of focus for several EDOF lenses with $f' = 125$ mm, $D = 4$ mm and $\lambda = 632.8$ nm.

linear to circular. There are two other pairs of polarizer and quarter-waveplate ($P_1 - QW_1$ and $QW_2 - P_2$), which form a state generator and a state analyzer, respectively. These elements are rotated until a phase modulation configuration is achieved since we want to study the behavior of a Fourier phase lens. After the state generator ($P_1 - QW_1$), the light goes through a 50:50 beam splitter, so that half of the light is directed to the SLM. We have used PLUTO Holoeye reflective LCoS modulator, which has a 1920 × 1080 resolution and a pixel size of 8 μm × 8 μm.

Then, the light reflected by the modulator passes again the beam splitter and is directed to the state analyzer ($QW_2 - P_2$). As shown in Fig. 8, between the plates of the analyzer there is a 4-f system in order to generate the SLM image near to the camera. We have used a 72BUC02-ML CMOS camera (Imaging Source Europe GmbH, Germany) with 2592 × 1944 pixels and a pixel size of 2.2 × 2.2 μm^2. Moreover, this camera is placed over a linear motor (Physik Instruments GmbH, Germany), which allows to move the camera in the beam propagation direction to study the behavior of the EDOF lenses. Furthermore, since the SLM introduces aberrations to the reflected beam, we have removed them adding an astigmatic phase map to the SLM.

First, we have analyzed the performance of the FSDL for lenses with $f' = 125$ mm, and $\Delta f = 12.5$ mm and $\Delta f = 25$ mm respectively. We sent our optimized DOF lenses to the SLM. Then, using the linear motor, we moved the camera around the focal position in order to calculate the FWHM for $f' - \Delta f/2 \leq z \leq f' + \Delta f/2$. Fig. 9 shows the results obtained for both lenses. In the case of the lens with $\Delta f = 12.5$ mm, the average FWHM is 43.63 μm, only 5.6 μm larger than the numerical value. Similarly, the FWHM curve of $\Delta f = 25$ mm is quite close to the theoretical one, reaching an average experimental beam width of 59.24 μm. For the experimental results, we have plotted the fitting, performed with kriging [33–35], and the 1σ and 2σ error bands in shading. In addition, we have determined the mean differences between experimental, $FWHM_{exp}(z)$, and numerical data, $FWHM_{num}(z)$, using

$$\Delta\sigma_{abs} = std\left[FWHM_{exp}(z) - FWHM_{num}(z)\right], \quad (21)$$
$$\Delta\sigma_{rel} = \frac{\Delta\sigma_{abs}}{\langle FWHM_{num}(z)\rangle},$$

where std is the standard deviation. For the lens with $\Delta f = 12.5$ mm, we have obtained $\Delta\sigma_{abs} = 6.7$ μm and $\Delta\sigma_{rel} = 13\%$, and for the lens with $\Delta f = 25$ mm, the values are $\Delta\sigma_{abs} = 10.6$ μm and $\Delta\sigma_{rel} = 17\%$.

Then, we compare the experimental beam width of FSDL with that of the SFZP and Lotus lenses for the cases $\Delta f = 12.5$ mm and $\Delta f = 25$ mm. Fig. 10 shows the experimental results of these three lenses. For both cases, the beam width at $z = f'$ increases significantly with respect to the width between $z = f' - \Delta f/2$ and $z = f' + \Delta f/2$ positions for SFZP and Lotus lenses. Nevertheless, the FSDL presents a more uniform intensity pattern and lower FWHM (red curve). For example, for $\Delta f = 25$ mm (Fig. 10b), the Lotus lens present an average beam width of 74.50 μm, the SFZP 73.50 μm, and the FSDL 59.70 μm, a 19.8% lower.

5. Conclusions

Lenses that produce a long, narrow, and uniform focal intensity distribution are of crucial importance in many fields of science and technology, such as imaging systems, intraocular lenses, or laser material processing. We present a new petal-shaped lens design, named Fourier Series Diffractive Lens (FSDL), whose focal length is defined as an angular Fourier series distribution. We have used Particle Swarm Optimization (PSO) algorithm to determine best Fourier coefficients in terms of the lens parameters (wavelength, focal length, depth of focus, diameter, number of petals) and Chirp Z-Transform (CZT) algorithm for a fast computation of the intensity distribution. The results

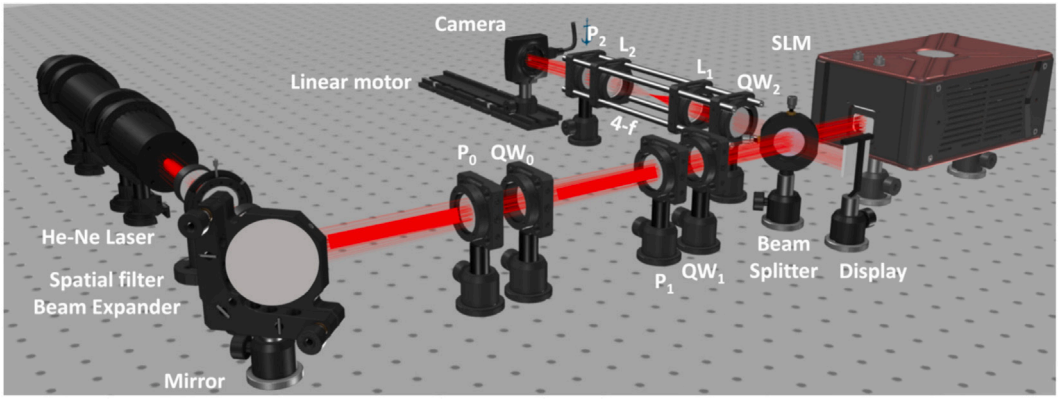

Fig. 8. Experimental set-up used to analyze the FSDL performance with a SLM. A motorized camera allows us to determine the beam parameters of the optimized FSDL around the focus.

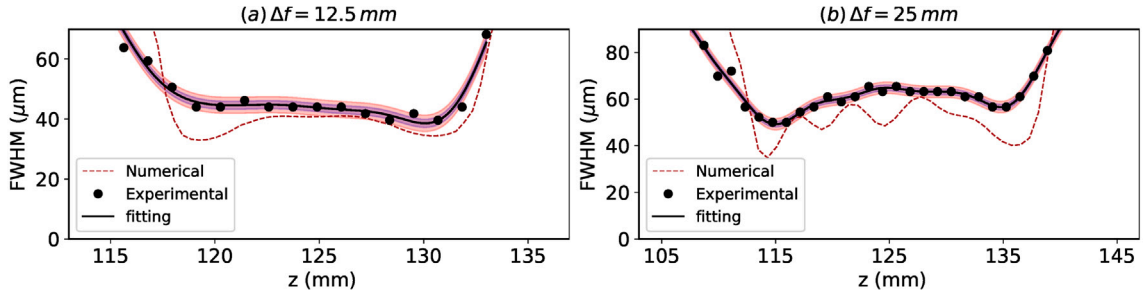

Fig. 9. Comparative between numerical and experimental FWHM for the Fourier lenses with $f' = 125$ mm, $D = 4$ mm, (a) $\Delta f = 12.5$ mm and (b) $\Delta f = 25$ mm. Also, we have included 1σ error bands (purple) and 2σ error bands (orange).

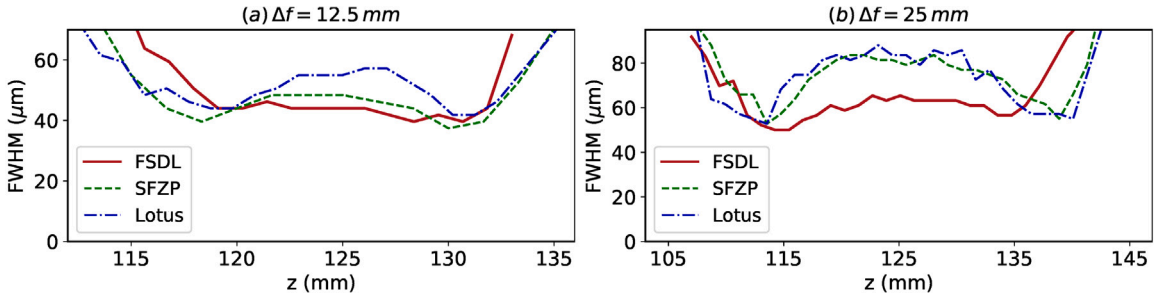

Fig. 10. Experimental beam width, calculated by FWHM approach, for FSDL, SFZP and Lotus lens with $f' = 125$ mm, $D = 4$ mm, (a) $\Delta f = 12.5$ mm and (b) $\Delta f = 25$ mm.

obtained with the FSDL have been compared with previous designs, such as Lotus lens and Sectorized Fresnel Zone Plate (SFZP). In all cases, FSDL presents a smaller beam width and better uniformity for a given depth of focus. In addition, we have studied how increasing the depth of focus affects the beam width, concluding that it presents a square root dependence. Finally, we have experimentally verified the performance of the FSDL using a Spatial Light Modulator (SLM) and a motorized camera determining the intensity distribution in the focal region. The experimental results are in good agreement with the numerical simulations, and verify better performance of the FSDL in comparison to previous designs. For example, for a lens with focal distance $f' = 125$ mm, and $\Delta f = 25$ mm the Lotus and SFZP lenses presents a average beamwidth of 74.5 μm and 73.5 μm, respectively while the FSDL results in 59.7 μm.

Declaration of competing interest

The authors declare that they have no known competing financial interests or personal relationships that could have appeared to influence the work reported in this paper.

Data availability

Data will be made available on request.

Acknowledgments

This work has been funded by project Retos Colaboración 2019 “Teluro” RTC2019-007113-3 of the Ministerio de Ciencia e Innovación and the European Union, European funds for regional development and from Plan Nacional de Investigación from Ministerio de Ciencia e Innovación: Nanorooms PID2019-105918GB-I00 and AL-LIO PID2021-122486OA-I00 projects.

References

[1] O. Lévêque, C. Kulcsár, A. Lee, H. Sauer, A. Aleksanyan, P. Bon, L. Cognet, F. Goudail, Co-designed annular binary phase masks for depth-of-field extension in single-molecule localization microscopy, Opt. Express 28 (22) (2020) 32426.

[2] Q. Fan, W. Xu, X. Hu, W. Zhu, T. Yue, C. Zhang, F. Yan, L. Chen, H.J. Lezec, Y. Lu, A. Agrawal, T. Xu, Trilobite-inspired neural nanophotonic light-field camera with extreme depth-of-field, Nature Commun. 13 (1) (2022).

[3] S.P. Murzin, N.L. Kazanskiy, C. Stiglbrunner, Analysis of the advantages of laser processing of aerospace materials using diffractive optics, Metals 11 (6) (2021) 963.
[4] F. Vega, M.S. Millán, M.A. Gil, N. Garzón, Optical performance of a monofocal intraocular lens designed to extend depth of focus, J. Refract. Surg. 36 (9) (2020) 625–632.
[5] P. Kanclerz, F. Toto, A. Grzybowski, J.L. Alio, Extended depth-of-field intraocular lenses: An update, Asia-Pacific J. Ophthalmol. 9 (3) (2020) 194–202.
[6] H.A. Weeber, S.T. Meijer, P.A. Piers, Extending the range of vision using diffractive intraocular lens technology, J. Cataract Refract. Surg. 41 (12) (2015) 2746–2754.
[7] T. Kohnen, R. Suryakumar, Extended depth-of-focus technology in intraocular lenses, J. Cataract Refract. Surg. 46 (2) (2020) 298–304.
[8] J. Ojeda-Castañeda, E. Yépez-Vidal, E. García-Almanza, Complex amplitude filters for extended depth of field, Photon. Lett. Poland 2 (4) (2010) 162–164.
[9] N. Davidson, A.A. Friesem, E. Hasman, Holographic axilens: High resolution and long focal depth, Opt. Lett. 16 (7) (1991) 523.
[10] W. Chen, C. Quan, C.J. Tay, Extended depth of focus in a particle field measurement using a single-shot digital hologram, Appl. Phys. Lett. 95 (20) (2009).
[11] L.A. Romero, M.S. Millán, Z. Jaroszewicz, A. Kołodziejczyk, Programmable diffractive optical elements for extending the depth of focus in ophthalmic optics, Proc. SPIE 9287 (January 2015) (2015) 92871E.
[12] S. Pinilla, S.R.M. Rostami, I. Shevkunov, V. Katkovnik, K. Egiazarian, Hybrid diffractive optics design via hardware-in-the-loop methodology for achromatic extended-depth-of-field imaging, Opt. Express 30 (18) (2022) 32633.
[13] R.G. Gonzalez-Acuña, J.C. Guitiérrez-Vega, Generalization of the axicon shape: The gaxicon, J. Opt. Soc. Amer. A 35 (11) (2018) 1915.
[14] H. Wang, C. Hao, H. Lin, Y. Wang, T. Lan, C.W. Qiu, B. Jia, Generation of super-resolved optical needle and multifocal array using graphene oxide metalenses, Opto-Electron. Adv. 4 (2) (2021) 200031.
[15] W. Daschner, B. Block, A. Thornton, B.C. Kress, Dual focus lens with extended depth of focus, U.S. Patent No. 6,330,118,1, 2001.
[16] B.C. Kress, P. Meyrueis, Applied Digital Optics: From Micro-Optics to Nanophotonics, John Wiley & Sons, 2009.
[17] A. Sabatyan, M. Golbandi, Petal-like zone plate: Long depth bifocal diffractive lens and star-like beam generator, J. Opt. Soc. Amer. A 35 (7) (2018) 1243.
[18] M. Golbandi, A. Sabatyan, Controlling and shaping topological charge by means of spiral petal-like zone plate, Opt. Laser Technol. 134 (2021).
[19] K. Uno, I. Shimizu, Dual focus diffractive optical element with extended depth of focus, Opt. Rev. 21 (5) (2014) 668–675.
[20] L.M. Sanchez-Brea, F.J. Torcal-Milla, J. del Hoyo, A. Cuadrado, J.A. Gomez-Pedrero, Optimization of angular diffractive lenses with extended depth of focus, J. Opt. 22 (2020) 065601.
[21] F.J. Torcal-Milla, L.M. Sanchez-Brea, J.A. Gomez-Pedrero, Sector-based Fresnel zone plate with extended depth of focus, Opt. Laser Technol. 154 (2022) 1–15.
[22] F. Zhou, R. Ye, G. Li, H. Zhang, D. Wang, Optimized circularly symmetric phase mask to extend the depth of focus, J. Opt. Soc. Amer. A 26 (8) (2009) 1890.
[23] P. Chen, X. Su, M. Liu, W. Zhu, Lensless computational imaging technology using deep convolutional network, Sensors 20 (9) (2020).
[24] J. Kennedy, R. Eberhart, B. Gov, Particle swarm optimization, in: Proceedings of ICNN'95-International Conference on Neural Networks, 1995, pp. 1942–1948.
[25] Y. Shi, R. Eberhart, Modified particle swarm optimizer, in: Proceedings of the IEEE Conference on Evolutionary Computation, ICEC, IEEE, 1998, pp. 69–73.
[26] H. Zappe, Fundamentals of Micro-Optics, Cambridge University Press, 2010.
[27] L.M. Sanchez-Brea, Diffractio, Python module for diffraction and interference optics, 2019, https://pypi.org/project/diffractio/.
[28] M. Leutenegger, R. Rao, R.A. Leitgeb, T. Lasser, Fast focus field calculations, Opt. Express 14 (23) (2006) 11277.
[29] Y. Hu, Z. Wang, X. Wang, S. Ji, C. Zhang, J. Li, W. Zhu, D. Wu, J. Chu, Efficient full-path optical calculation of scalar and vector diffraction using the Bluestein method, Light: Sci. Appl. 9 (1) (2020).
[30] F. Shen, A. Wang, Fast-Fourier-transform based numerical integration method for the Rayleigh-Sommerfeld diffraction formula, Appl. Opt. 45 (6) (2006) 1102–1110.
[31] L.J.V. Miranda, PySwarms: A research toolkit for particle swarm optimization in Python, J. Open Source Softw. 3 (21) (2018) 433.
[32] W.J. Smith, Modern Optical Engineering: The Design of Optical Systems, McGraw-Hill Education, 2008.
[33] N. Cressie, Statistics for Spatial Data, John Wiley & Sons, 2015.
[34] R. Christensen, Linear Models for Multivariate, Time Series, and Spatial Data, Vol. 1, Springer, 1991.
[35] L.M. Sanchez-Brea, E. Bernabeu, Determination of the optimum sampling frequency of noisy images by spatial statistics, Appl. Opt. 44 (16) (2005) 3276–3283.